

Fabrication of Scaffolds with a Hexagonal Array of Interconnected Pores (SHAIPs) as a Cell Delivery Platform for Tendon-to-Bone Repair

A Thesis Presented to
The Academic Faculty

By

Fred Lee

In Partial Fulfillment
of the Requirements for the Degree
Master of Science in Biomedical Engineering
Wallace H. Coulter Department of Biomedical Engineering

Georgia Institute of Technology

May 2025

Copyright © 2025 by Fred Lee

Fabrication of Scaffolds with a Hexagonal Array of Interconnected Pores (SHAIPs) as a
Cell Delivery Platform for Tendon-to-Bone Repair

Approved by:

Dr. Younan Xia, Advisor
Wallace H. Coulter Department of Biomedical Engineering
*Georgia Institute of Technology and
Emory University*

Dr. Edward A. Botchwey
Wallace H. Coulter Department of Biomedical Engineering
*Georgia Institute of Technology and
Emory University*

Dr. Vahid Serpooshan
Wallace H. Coulter Department of Biomedical Engineering
*Georgia Institute of Technology and
Emory University*

Date Approved: April 28, 2025

ACKNOWLEDGEMENTS

I express my deepest gratitude to my research advisor, Dr. Younan Xia, whose expertise helped guide my research and provided all the necessary funding to make this project possible. I am especially appreciative of Dr. Stavros Thomopoulos' group at Columbia University—namely, PhD candidates Ismael Bousso and Andrew Luzzi, as they provided the methodology and data for the cellular evaluation of the inverse opal scaffolds. Lastly, special thanks go to my postdoctoral advisor, Dr. Min Hao, and my colleagues in the Xia Group at the Georgia Institute of Technology for their valuable feedback and support throughout this undertaking.

TABLE OF CONTENTS

ACKNOWLEDGEMENTS.....	iii
LIST OF FIGURES.....	vi
LIST OF ABBREVIATIONS.....	vii
SUMMARY.....	viii
CHAPTER 1: INTRODUCTION.....	1
1.1. Scaffold Fabrication Techniques.....	2
1.1.1. Inverse Opal.....	3
1.1.2. Electrospinning.....	4
1.1.3. 3D Bioprinting.....	6
1.1.4. Decellularized Extracellular Matrix.....	9
1.2. Gli1 Activation in Tendon-to-Bone Regeneration.....	10
1.3. Study Overview.....	11
CHAPTER 2: METHODOLOGY.....	13
2.1. Materials.....	14
2.2. Microfluidic Emulsion.....	14
2.3. SHAIP Fabrication.....	17
2.4. Cell-Seeded Scaffold Characterization.....	18
2.4.1. In Vitro Evaluation.....	18
2.4.2. In Vivo Evaluation.....	19
CHAPTER 3: RESULTS AND DISCUSSION.....	20
3.1. Gelatin Microsphere Preparation.....	21

3.2. Gelatin Template Formation.....	24
3.3. SHAIP Fabrication.....	25
3.4. In Vitro Evaluation.....	27
3.5. In Vivo Evaluation.....	29
CHAPTER 4: CONCLUSIONS.....	31
CHAPTER 5: RECOMMENDATIONS.....	32
APPENDIX A: EXTRA FIGURES.....	33
REFERENCES.....	34

LIST OF FIGURES

Figure 1. Schematic of Simple Microfluidic Device.....	15
Figure 2. Graphical Overview of the Modified SHAIP Fabrication Method.....	18
Figure 3. Optical Micrographs of Gelatin Microspheres.....	23
Figure 4. Optical Micrographs of Thermal Annealing Outcomes.....	25
Figure 5. Optical Micrographs of Step-by-Step SHAIP Fabrication.....	27
Figure 6. Live/Dead Staining and <i>In Vitro</i> Gene Expression.....	28
Figure 7. Histological Analysis and <i>In Vivo</i> Gene Expression.....	30
Figure A1. Optical Micrographs of Coalesced Gelatin Microspheres.....	33
Figure A2. Optical Micrographs of Step-by-Step Bilayer Fabrication.....	33

LIST OF ABBREVIATIONS

2D	Two-dimensional
3D	Three-dimensional
ANOVA	Analysis of variance
CAD	Computer-aided design
CT	Computed tomography
dECM	Decellularized extracellular matrix
DI	Deionized
ECM	Extracellular matrix
Hh	Hedgehog
HhAg	Hedgehog agonist
LSD	Least significant difference
MRI	Magnetic resonance imaging
MSC	Mesenchymal stem cell
PCL	Polycaprolactone
PLGA	Poly(lactic-co-glycolic acid)
PVC	Poly(vinyl chloride)
rBMSC	Rat bone marrow-derived stem cell
RT-qPCR	Reverse transcription quantitative polymerase chain reaction
SHAIP	Scaffold with a hexagonal array of interconnected pores
SLRP	Small leucine-rich proteoglycans

SUMMARY

The use of monolayer inverse opal scaffolds, conventionally known as SHAIPIs, had been proposed as a cell delivery platform for HhAg-stimulated stem cells to improve tendon-to-bone healing outcomes in rotator cuff repair. SHAIPIs possess a well-defined pore structure and high pore interconnectivity, but these scaffolds have limited relevance in tissue engineering applications due to their complex fabrication process and poor scalability. This research explored a modified SHAIPI fabrication procedure based on traditional inverse opal scaffold techniques that offered greater scalability and solely depended on readily available laboratory equipment. The study was split into three main sections: monodisperse microsphere preparation, SHAIPI fabrication, and cell-seeded scaffold characterization. Uniform gelatin microspheres were obtained by optimizing the experimental parameters of a microfluidic emulsion procedure, which provided a reliable source of templating beads for SHAIPI fabrication. Furthermore, this modified SHAIPI fabrication procedure enabled the simultaneous production of multiple gelatin templates, addressing the bottleneck of the original process. Although the heating duration required for sufficient thermal annealing increased, large batches of these templates could be produced in a single trial, enhancing overall process throughput and scalability. rBMSCs were seeded into the resultant PCL SHAIPIs and then primed with HhAg for cell-seeded scaffold characterization to confirm viability as a cell delivery platform in tendon-to-bone regeneration. No apparent signs of cytotoxicity were observed when assessed via live/dead staining. Moreover, seeded HhAg-stimulated rBMSCs showed upregulated Gli1 expression relative to *in vitro* controls, comparable to previous studies on HhAg-stimulated MSCs that demonstrated improved enthesis healing. Ultimately, the histological analysis of the *in vivo* rat model illustrated the successful delivery of primed rBMSCs to the repair site, validating the feasibility of SHAIPIs as a cell delivery platform.

CHAPTER 1

INTRODUCTION

Tissue engineering is an interdisciplinary field with the objective to repair diseased or damaged tissues, restoring functionality by facilitating wound-healing processes. Scaffolds are a crucial element of tissue regeneration, as these structures provide mechanical support for and guide cellular growth. Scaffolds replace the function of the native tissue ECM and vary based on the intended application, designed to be as closely biomimetic to the original tissue as possible.^[1,4] Scaffold design is consistently progressing with the development of new biomaterials and fabrication techniques, encompassing far beyond the biochemical, mechanical, and physical properties of the scaffold structure. Additional scaffold parameters that are vital to successful cell growth and maturation include: porosity, pore interconnectivity, biodegradability, and architecture.^[3,4] Some studies focus on the advancement of cell-based scaffold-free tissue engineering approaches to avoid possible complications from the presence of foreign or artificial biomaterials. Unfortunately, while cells possess high therapeutic potential against many health conditions, current cell-based therapies have shown greatly limited effectiveness.^[5,6] Intra-tissue or intravenous injection are the most common cell delivery routes, but less than 5% of infused cells remain at the injection site within the first day of treatment, confirmed across multiple applications.^[5] Another standard cell-based scaffold-free tissue engineering approach relates to cell sheets, which emphasize effective cell-cell and cell-ECM communication. These microtissues have undergone significant improvement, capable of thoroughly recapitulating 2D tissue architecture. Recent developments in this cell sheet technology have also produced multi-layered 3D tissue assemblies, but similar limitations regarding the application of these cell sheets have held firm throughout the years.^[5] For example, production

processes are both time-consuming and largely restricted due to inadequate cell sourcing.^[4,5] Furthermore, these cell sheets are extremely fragile, and multi-layered cell sheets are susceptible to delamination and necrosis. By contrast, scaffold-based approaches are more robust, featuring improved reproducibility and scalability by providing a well-defined microenvironment for cells to thrive and proliferate.^[1,5] Scaffolds can also undergo extensive modification to tune various material compositions and characteristics such as the mechanical properties, enabling use across a wide range of fields and applications.

1.1. Scaffold Fabrication Techniques

Scaffold properties are directly linked to the biomaterial quality and processing method. Ideally, the scaffold will be biomimetic to the native tissue or organ, and process parameters will be optimized for that specific application. For example, the scaffold degradation rate can be finely tuned to be synonymous with the tissue growth rate, maintaining sufficient structural integrity and if needed, load-bearing capabilities throughout the lifetime of the device.^[2,6] Moreover, the degradation products must be non-toxic and manageable for cells either through metabolism or excretion. Basic scaffold requirements are high biocompatibility and cell viability. Each scaffold fabrication technique has distinct advantages and limitations, offering precise control over select scaffold parameters while proving less effective for other properties. Despite continuous developments in scaffold fabrication techniques, only methods with high scalability, translatability to clinical studies, or both are pertinent to further research and funding.^[1,7] Four widespread scaffold fabrication techniques include: inverse opal, electrospinning, 3D bioprinting, and dECM. This study expands on scaffold fabrication using the inverse opal method.

1.1.1. Inverse Opal

Inverse opal scaffolds inherit the characteristics of a template formed from a closely-packed lattice of uniform microspheres. The inverse opal method can be split into five main steps: lattice formation, microsphere necking, template collection, polymeric infiltration, and selective template removal. Once the closely-packed lattice is arranged through various strategies, the templating microspheres are connected to form channels that hold the template together and shape the interconnecting windows between pores in the final scaffold structure. The polymer solution penetrates the void spaces of this template and solidifies, and then the template is removed without disrupting the polymer material. Scaffolds produced through this fabrication method possess high uniformity with a well-defined 3D structure and network of pores, featuring high porosity and pore interconnectivity based on the templating microspheres.^[8,9] As these inverse opal scaffolds adopt the template qualities, the pore size can be realistically varied between 50-1000 μm to fit the intended application and target cell type.^[10] For example, the optimal pore size for bone tissue engineering lies between 100-250 μm .^[8] In addition, this uniform scaffold structure facilitates even cell distribution which is a common problem encountered when seeding 3D constructs, further improving scaffold consistency and bioactivity. The well-regulated pore size and interconnectivity, which is approximately 15-25% of the scaffold pore size, promotes cell migration and the diffusion of nutrients, waste, and oxygen throughout the bulk scaffold structure.^[10] Notably, the high pore interconnectivity encourages active cell signaling that expedites cell growth and tissue remodeling, improving the integration of the regenerated tissue into the patient. The ample void space in this pore arrangement also prompts the formation of neovasculature, another key element of wound healing.^[11,12] Moreover, this scaffold fabrication technique is precise and reproducible, enabling the collection of more clinically translatable results from *in vitro* and *in vivo* testing. Conversely, although

high porosity can be achieved through conventional scaffold fabrication approaches, the pore distribution is typically heterogeneous with irregular pore sizes and uncontrolled interconnectivity. For example, solvent leaching procedures can create scaffolds with up to 90% porosity, but this method demonstrates limited control over pore formation.^[7] Consequent scaffolds acquire unpredictable pore distributions with high batch-to-batch variation. Furthermore, this alternative process is time-consuming, requires extensive post-processing to remove hazardous chemical residues, and possesses limited use in cell studies. Inverse opal scaffolds exhibit strong mass transport capabilities and a consistent, well-defined microenvironment that promotes cell proliferation, growth, and differentiation. Similar to the monodisperse microspheres used in templating, these uniform scaffold properties are also suitable carriers for long-term controlled drug delivery.^[13,14] Recent studies on inverse opal drug delivery mechanisms have identified the color-changing capabilities of these scaffolds when releasing the incorporated drugs, which can be easily detected using a spectrophotometer for the real-time monitoring of drug release.^[15,16] Unfortunately, a considerable disadvantage of this inverse opal method centers around the difficulty in fabrication and scale-up of large 3D scaffolds. This fabrication method also struggles with the production of non-spherical pores that are more suitable for certain biomedical applications such as nerve and soft tissue regeneration.^[11] The inverse opal method is a highly versatile technique for the production of uniform scaffolds with high porosity and pore interconnectivity, suitable for cell studies on small tissue regeneration and tissue interfaces.

1.1.2. Electrospinning

Nanofibrous scaffolds are assembled through the deposition of electrospun nanofibers, forming mats that closely resemble the native ECM structure, which is primarily composed of various fibrous structural proteins such as collagen and fibrin.^[1,2]

Electrospinning is a conventional technique for producing homogeneous nanofibers with finely-tuned physical and chemical properties from a wide range of materials—particularly polymeric biomaterials. By applying a high-voltage current to the polymer solution, the droplet at the needle tip overcomes surface tension, forming a Taylor cone that then generates a continuous stream of nanofibers. The nanofibrous scaffolds are prepared through the deposition of these electrospun nanofibers, which can be arranged into various patterns by adjusting the collection method.^[17,18] This arrangement significantly influences the scaffold's topographical features, physicochemical properties, and reported cell behavior. For example, uniaxially-aligned fibers promote cell migration and directional growth along the length of the fibers, whereas radially-aligned fibers improve cellular infiltration into the central scaffold region.^[17] This fabrication technique enables the high-throughput production of reproducible scaffolds with high porosity and pore interconnectivity. Moreover, based on the nanofiber arrangement, the scaffold uniformity and surface topography can be tailored to meet the morphological and functional specifications of the target tissue. In skin tissue engineering, the randomly-oriented nanofiber mats provide the most evenly distributed mechanical properties, supporting uniform cell growth, whereas uniaxially-aligned nanofiber scaffolds promote directional physical characteristics that guide cell elongation for proper matrix alignment.^[17] Limitations of these nanofiber mats include small pore sizes, limited diffusion capacity, and low mechanical strength. Although the scaffold pore size can be controlled by changing the electrospinning parameters, the pore size is limited to 5-35 μm , accounting for possible post-process modifications for pore enlargement.^[1,18] Despite possessing high pore interconnectivity, their small pore size significantly restricts their diffusion capacity. Consequently, their suboptimal diffusion capacity can lead to complications regarding cell viability and behavior due to insufficient nutrient supply and the excessive build-up of waste products. While scaffolds are designed to degrade into non-toxic

byproducts, the insufficient removal or metabolism of these degradation products can inhibit normal wound-healing processes. For example, although PLGA degrades into lactic and glycolic acid, both of which are non-toxic and can be metabolized or eliminated from the regenerated tissue, high concentrations of these byproducts can significantly reduce the local pH, inhibiting cell proliferation, communication, and normal protein activity.^[6] Additionally, the high porosity and loosely-packed fibers of electrospun mats lead to low mechanical strength unless supplementary crosslinking procedures are applied to the composite nanofibers. Nanofibrous scaffolds are frequently denoted as mats since this fabrication technique is limited to the creation of 2D and extremely thin 3D structures. Their low mechanical properties are unable to support larger constructs, and crosslinking processes can significantly alter the properties of the constituent biomaterials.^[7] The shared capacity for precise control over pore size and distribution between electrospinning and the inverse opal method prompt similarities in applications, such as sustained drug release. Regrettably, although electrospinning provides considerably higher throughput and scalability than the inverse opal method, the small pore size and poor mechanical strength of electrospun mats diminish the clinical potential of this technique in scaffold fabrication. Specifically, the use of electrospun mats for cell delivery applications was deemed surgically unfeasible, as they immediately split apart when attempts were made to suture the scaffold to the repair site. Nevertheless, electrospinning is a multifaceted technique for preparing homogeneous nanofibers, which are commonly incorporated into composite materials for enhanced bioactivity, drug delivery, and wound healing.^[3,17]

1.1.3. 3D Bioprinting

3D bioprinting is the layer-by-layer fabrication of 3D scaffold structures based on a processed CAD model, conventionally understood as the extrusion-based approach.

This fabrication technique can be roughly divided into three steps: designing, printing, and post-processing. In the designing stage, the CAD model is generated using various medical imaging systems such as MRI or CT and then sliced into thin, printable layers for the bioprinter. If necessary, supplementary details and support structures are added at this stage. Alternatively, the CAD model can be separately designed with certain features or characteristics needed to fit an application based on prior research or clinical data. Following model refinement, the printing phase is closely monitored to address any potential errors in the extruded structure, which ensures high print fidelity relative to the intended model. This printed 3D construct is subsequently stabilized through various mechanisms, with photocrosslinking being the standard approach.^[1,19] Post-processing prepares the structure for use or scaffold characterization by removing any unwanted support material and when applicable, seeding cells. Scaffolds produced using 3D bioprinting exhibit high structural fidelity, scalability, and reproducibility. This technique is commonly implemented in bone tissue engineering due to high spatial resolution, which allows the formation of complex geometries with controlled pore size and pore interconnectivity that mimic natural bone tissue architecture.^[4,19] Furthermore, since 3D bioprinting frequently relies on CAD models reconstructed from medical imaging data, the printed scaffolds can be specifically tailored to provide an exact fit for the target tissue or injury site. A widely recognized benefit of 3D bioprinting is the creation of a well-defined network of vasculature, which remains a prevalent issue across most 3D tissue models.^[2,19] Additionally, printed scaffolds can avoid cell-seeding complications, as these cells can be directly incorporated into the bioink, which leads to an even cell distribution throughout the scaffold structure.^[19] Recent developments in bioprinters also enable the accurate replication of cell layers by alternating between multiple bioinks. The main disadvantages of 3D bioprinting relate to the substantial equipment costs, limited bioink selection, and slow printing speed. Although extrusion-based bioprinters are the

most affordable devices among standard bioprinting methodologies, this technology remains inaccessible for most standard laboratories. Moreover, the spatial resolution of this approach is generally limited to 200 μm , which may reduce the broader applicability of this technique.^[20] In addition, the available selection of materials suitable for 3D bioprinting are limited, requiring specific shear-thickening and shear-thinning fluid properties. Cells, which are regularly incorporated into these bioinks, will experience strong shear forces during this printing process that can change cell behavior and functionality.^[3,19] Therefore, although some applications such as soft tissue engineering can directly produce cell-laden structures, the separate seeding of acellular scaffolds remains widespread for most 3D bioprinting applications. Furthermore, the layer-by-layer fabrication found in extrusion-based approaches leads to exceedingly slow printing speeds, which renders this process unsuitable for large 3D structures.^[3] Despite the high spatial fidelity characteristic of bioprinted scaffolds, 3D bioprinting requires expensive machinery, whereas inverse opal scaffolds can be fabricated in any laboratory with basic material processing capabilities. Moreover, although extrusion-based bioprinting can achieve a uniform pore size and distribution, the formation of the well-defined lattice of interconnected pores observed in inverse opal scaffolds is challenging. Inadequate spatial resolution and variable material properties can compromise the fidelity of this bioprinted network of pores, particularly for pore sizes below 200 μm . Bioink is highly sensitive to external factors such as temperature, humidity, and bioprinter stability, which can lead to variability in material properties during the printing process. In the fabrication of the closely-packed hexagonal pore arrangement, the simplicity of the inverse opal method enables the formation of scaffolds with more consistent mechanical and physical properties, thereby enhancing reproducibility and clinical translatability. This elevated scaffold consistency is crucial for accurately assessing treatment effectiveness when used as a cell delivery platform in tendon-to-bone regeneration. The high spatial control

and reproducibility of bioprinted scaffolds has seen extensive use in disease modeling, but this technique is currently restricted to the fabrication of complex, smaller tissues.^[19] As additional research is conducted to improve the accessibility of 3D bioprinting and expand the range of available bioinks, this technique can be expanded to a wider array of applications.^[6,20]

1.1.4. Decellularized Extracellular Matrix

dECM scaffolds strongly recapitulate the native tissue environment, achieving the biomimetic goal of scaffold design: to recreate and replace the function of the native ECM. The preparation of dECM scaffolds relies on the complete removal of cellular components from the tissue-specific ECM using various decellularization processes that depend on a broad range of physical, chemical, and enzymatic techniques. No single, optimal decellularization method has been identified due to tissue-specific ECM characteristics, which exhibit varying responses to applied treatments. Instead, a combination of all three approaches has been shown to best preserve the ECM architecture, biochemical composition, mechanical properties, and bioactive molecule integrity.^[4] Unsuitable decellularization processes can alter the biochemical and physical properties of the ECM, leading to structural degradation and reduced cell viability.^[4,12] Incomplete decellularization also results in significant issues regarding immunogenicity, where residual cellular material can induce a foreign body response. dECM scaffolds exhibit high biocompatibility and bioactivity, closely matching the native tissue architecture, composition, and mechanical properties. Moreover, dECM contains large quantities of biochemical cues that recapitulate the tissue microenvironment, including some unknown components. Unfortunately, while dECM is a highly versatile biomaterial, challenges in mechanical stability and production reduce the applicability of dECM as a scaffold fabrication technique. Specifically, dECM is extremely fragile and possesses low

mechanical strength, necessitating crosslinking before use as a scaffold, which may change the native ECM properties. ECM sourcing is another major obstruction in the clinical application of dECM. Typically sourced allo- or xenogenically, slight variations in tissue architecture between the donor and patient can lead to immunogenic complications.^[4] Although dECM can be sourced autogenically via ECM deposition of *in vitro*-cultured cells, securing a sufficient amount is time-consuming and impractical.^[4,5] Instead, dECM is commonly incorporated into other biomaterials, serving as a reservoir of bioactive molecules that promote cell communication, differentiation, and viability. For example, solubilized dECM has been incorporated into bioinks for bone tissue regeneration to enhance biocompatibility, facilitate cell growth, and promote tissue remodeling.^[12,17] Regardless, the overall scalability of this process is limited due to restricted ECM supply and unreliable sourcing. Relative to inverse opal scaffolds, dECM scaffolds possess superior biomimetic capabilities but exhibit poor reproducibility, which limits their clinical potential. Their high batch-to-batch variability from inherent tissue heterogeneity and lack of process standardization obscures treatment effectiveness when used as a cell delivery platform. dECM scaffolds can effectively reproduce the native tissue architecture and microenvironment, enhancing natural wound-healing processes; however, further research is needed to improve material availability and consistency for clinical translation.

1.2. Gli1 Activation in Tendon-to-Bone Regeneration

Rotator cuff tears are common shoulder injuries that often cause severe pain and reduced mobility from impaired shoulder function. These injuries are normally treated using surgical methods, but the postoperative failure rate of rotator cuff repair remains exceptionally high, reportedly reaching retear rates of up to 94% in long-term follow-up studies.^[21] Post-treatment failures are frequently linked to the inadequate regeneration of

the enthesis, a specialized connective tissue that attaches the tendon to bone. Prior research by Dr. Stavros Thomopoulos has shown that Hh-responsive Gli1+ stem cells promote proper enthesis development, exhibiting enthesis-specific stem cell properties.^[22,23] The Hh-signaling pathway regulates cell proliferation, differentiation, and migration, each contributing to optimal tissue regeneration and maturation. Gli1 is a key downstream transcription factor in the Hh-signaling pathway and serves as a marker for pathway activation. After cells are stimulated using HhAg, Gli1 expression increases, leading to the differentiation of MSCs into fibrocartilaginous and osteogenic lineages. Gli2 and Gli3 are mediators that can activate or repress Gli1 expression, with Gli3 functioning primarily as a repressor. Although Gli2 is also an active form of the Gli proteins, it is associated with various other roles and signaling pathways, whereas Gli1 more consistently reflects Hh-pathway activation.^[23] Considering the significance of this pathway in tissue regeneration, this study aims to deliver Gli1+ stem cells to the tendon-to-bone repair site, enhancing enthesis healing outcomes.

1.3. Study Overview

Expanding on the delivery of Gli1+ stem cells, this study focuses on the validation and scale-up of inverse opal scaffold fabrication techniques for use as a cell delivery platform in tendon-to-bone repair. Specifically, this study modifies the SHAIIP production process, a subset of inverse opal scaffolds consisting of a single layer. Retaining the uniform pore distribution and high pore interconnectivity of inverse opal scaffolds, SHAIIPs can form thin, homogeneous scaffolds suitable for superficial wounds and tissue interfaces.^[10,15] For example, inverse opal scaffolds have been widely used in enthesis regeneration to facilitate the gradual integration of tissues at the interface, driven by enhanced cell communication, migration, and nutrient diffusion.^[24] Previous studies on SHAIIP fabrication primarily covered a proof-of-concept demonstration of a

specialized fabrication approach, supported by preliminary data collected from short-term *in vitro* and *in vivo* cell studies.^[10] Although successful SHAIP fabrication was observed, this method demonstrated low throughput, with only a small number of trials performed. Here, I implemented and optimized a modified SHAIP fabrication procedure based on the standard inverse opal method to increase process scalability and clinical relevance. Cell-seeded scaffold characterization data was provided by Dr. Stavros Thomopoulos' group at Columbia University, evaluating the feasibility of PCL SHAIPs as a cell delivery platform for enthesis repair.

CHAPTER 2

METHODOLOGY

This section provides an overview of the methodology used in SHAIIP fabrication and evaluation, with detailed procedural steps described in subsequent subsections. First, monodisperse gelatin microspheres were obtained through a microfluidic emulsion procedure and then freeze-dried to help preserve their structural integrity. These dried microspheres were arranged into a closely-packed hexagonal lattice and connected together via thermal annealing. Once cooled to room temperature, the template was infiltrated using 10% PCL in dichloromethane, where the polymer solution was frozen and then lyophilized in the void spaces of the template. The templating material, gelatin, was removed by gently heating the template-containing scaffold in DI water at 40 °C.

HhAg-stimulated rBMSCs were seeded onto the resultant PCL SHAIIPs to test their viability as a cell delivery platform for entheses regeneration through various *in vitro* and *in vivo* evaluations. Scaffold cytotoxicity was determined via live/dead staining, and gene expression was measured using RT-qPCR. Genetic expression profiles were compared to their respective *in vitro* controls to gauge changes in cellular response. Finally, histological analysis of DI-I labeled rBMSCs was used to assess the delivery of primed rBMSCs to the repair site. All cellular research presented in this study was conceptualized and performed by Dr. Stavros Thomopoulos' group at Columbia University.

2.1. Materials

Gelatin (type A, from porcine skin), sorbitan monooleate (Span® 80), and toluene ($\geq 99.5\%$) were used to prepare monodisperse gelatin microspheres through microfluidic emulsion. Methanol ($\geq 99.8\%$) was used to wash and store the stabilized microspheres in suspension, which further increased long-term structural integrity. Gelatin templates were infiltrated with PCL in dichloromethane ($\geq 99.8\%$) for the fabrication of SHAIPs. All materials for SHAIIP fabrication were obtained from Sigma-Aldrich and used as received.

2.2. Microfluidic Emulsion

Uniform gelatin microspheres were produced through microfluidic emulsion using a simple microfluidic device fabricated according to a previously published procedure.^[13] The microfluidic device was composed of a PVC tube (ID: 0.7 mm, OD: 2.4 mm), glass capillary (ID: 0.55 mm, OD: 0.95 mm), and syringe needles as illustrated in Figure 1. 30G and 18G needles were used for the discontinuous and continuous phases, respectively. The device was sealed with epoxy glue and then left undisturbed for at least 24 h before use. Ideally, the continuous phase applied a sufficient force to the discontinuous phase droplet at the needle tip to establish a dripping flow pattern for the production of uniform microspheres. Insufficient forces caused incomplete droplet separation, resulting in the fabrication of small particles in addition to the intended microspheres, thus increasing sample polydispersity. A mismatch in the discontinuous and continuous phase flow rates could lead to jetting, where the discontinuous phase broke apart at some distance from the needle tip, generating non-uniform microspheres due to unstable droplet formation (Figure 1).^[14]

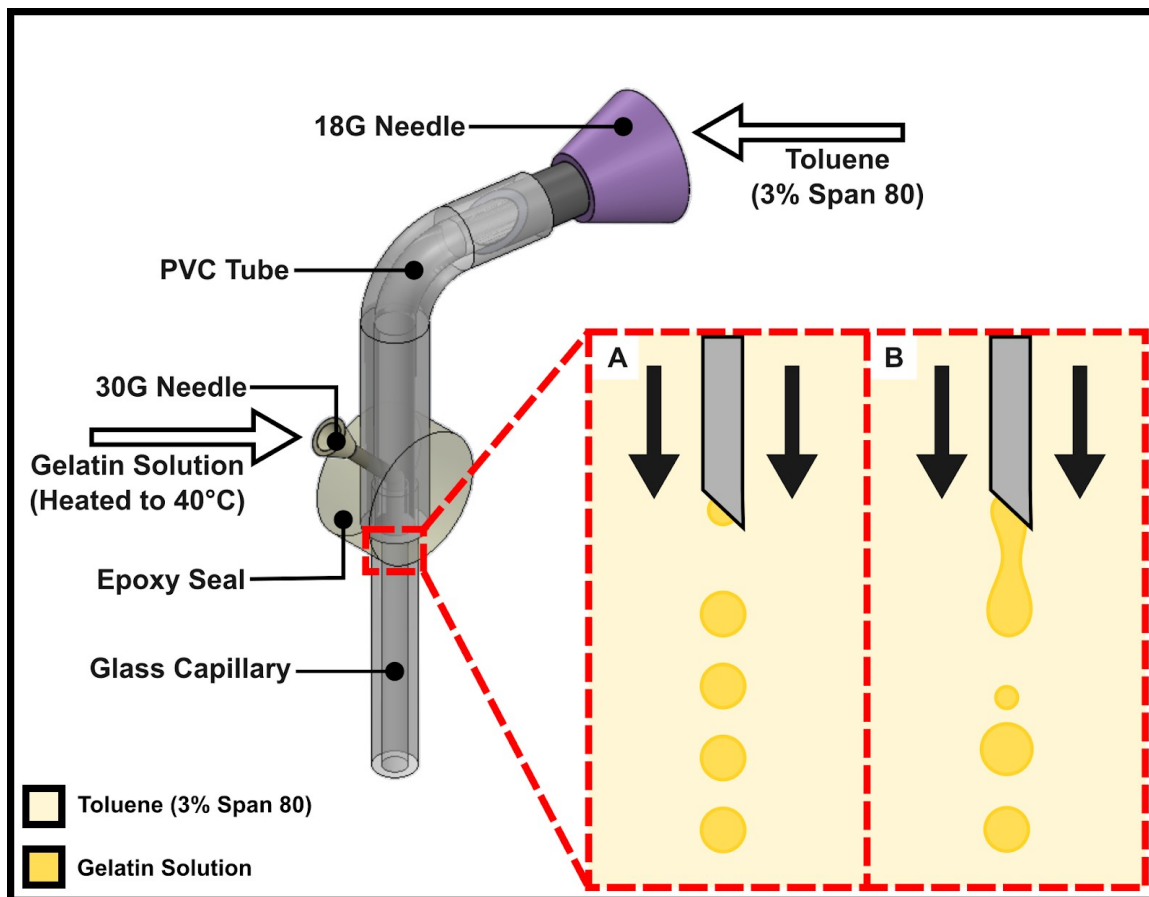


Figure 1. Schematic of simple microfluidic device with supplementary diagrams describing commonly observed flow patterns: (A) dripping and (B) jetting, respectively.

Gelatin microspheres were produced using an aqueous gelatin solution heated to 40 °C as the discontinuous phase, with toluene containing Span 80 (3%) as the continuous and collection phases. Once prepared, the solutions were allowed to rest with little to no agitation for at least 12 h before microfluidic bead preparation, passively degassing the solutions to prevent any possible disruptions to steady fluid flow in the device. The collection phase was agitated at 200 RPM and cooled in an ice bath for at least 30 min prior to microsphere fabrication to prevent bead aggregation and to stabilize the generated droplets. Uniform gelatin microspheres were obtained using 20% gelatin at 0.0375 and 0.75 mL/min for the discontinuous and continuous phase flow rates, respectively. The syringe pump for the continuous phase was started before and stopped after that of the discontinuous phase, where the microfluidic device output was isolated for 3 min upon the initial observation of microspheres as the system stabilized. Once microsphere production concluded, the collection phase was cooled for the next 4 h, and the toluene was allowed to fully evaporate over 4-5 days until the collection phase became clear. The gelatin microspheres were thoroughly washed with methanol three times and then stored in suspension using fresh methanol. A thin layer of these microspheres was evenly spread across a dish containing a small amount of methanol and then frozen at -80 °C for 1 h. Once thoroughly cooled, the gelatin microspheres were dried under vacuum for at least 24 h before use for templating to help preserve bead structural integrity during the thermal annealing process. Upon drying, gelatin microspheres transition from a white, translucent appearance to a golden-yellow color. The dried gelatin microspheres are similarly stored in a methanol suspension to improve long-term stability and prevent unexpected structural degradation.

2.3. SHaip Fabrication

PCL SHaipS were prepared using a modified procedure based on the production of traditional inverse opal scaffolds (Figure 2).^[10,11] A methanol suspension of uniform gelatin microspheres was carefully dropped onto the conical wall of a 50 mL centrifuge tube until the flat circular base was completely covered by a monolayer of the uniform microspheres. Once a sufficient number of microspheres were loaded, 5 mL of methanol was introduced, and the centrifuge tube was sealed and then sonicated for 10 s. The loosely-packed microspheres were arranged into a closely-packed hexagonal lattice using the vertical tapping method, where the bottom of the centrifuge tube was gently tapped periodically for 3 min. Smaller microspheres less than 100 μm required a prolonged tapping duration to ensure that the beads were properly arranged. After the lattice became clearly defined, the centrifuge tube was carefully placed in a box oven at 80 °C for 4 h to induce thermal annealing of the gelatin microspheres, creating the inverse opal template. When the template cooled to room temperature, the tube was unsealed, and excess methanol was removed without disrupting the template structure. The remaining methanol was left to evaporate in a fume hood. Once sufficiently dried, the template was easily released and collected from the centrifuge tube mold. The template was meticulously placed on a filter paper using a spatula to allow any residual methanol to fully evaporate overnight. The void spaces throughout the gelatin template were infiltrated with 10% PCL in dichloromethane by wiping off any excess polymer solution from the template surface using filter paper. This infiltrated template was frozen at -20 °C for 5 h and then lyophilized for at least 12 h. Thereafter, the freeze-dried sample was submerged in ethanol for 2 min under vacuum and then transferred into a container of DI water. The template-containing scaffold was heated to 40 °C for 3 h with minimal agitation to gradually dissolve the templating gelatin microspheres while preserving the SHaip structure.

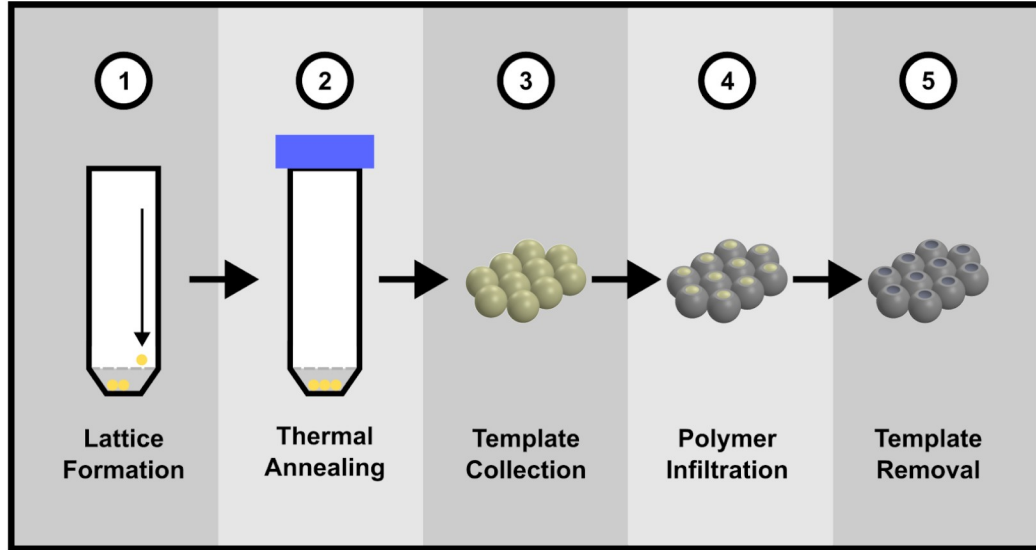


Figure 2. Graphical overview of the modified SHAIP fabrication method.

2.4. Cell-Seeded Scaffold Characterization

PCL SHAIPs with a uniform pore size of 190 μm , suitable for enthesis regeneration, were incorporated into all subsequent scaffold-based experiments. Cell studies were conducted using rBMSCs isolated from the femur and tibia of Sprague-Dawley rat bone marrow. The genetic expression profiles for all cell populations were conducted using RT-qPCR, a widespread technique for measuring gene expression levels due to high sensitivity and quick speeds. Following the methods described by Dr. Stavros Thomopoulos, RT-qPCR data was analyzed for significance using ANOVA with an LSD post hoc test, where $p < 0.05$ was considered significant.

2.4.1. *In Vitro* Evaluation

Preliminary tests were performed on the PCL SHAIPs to assess feasibility as a cell delivery platform for HhAg-stimulated stem cells in enthesis regeneration. rBMSCs were seeded onto the SHAIPs and primed with 0.5 μM HhAg for 4 and 14 days, respectively. Gene expression levels for Gli1 and downstream tendon enthesis markers

(Scx, Sox9, Runx2, Dcn, and Bgn) of the primed rBMSCs were compared against non-stimulated controls at 4 and 14 days. Additionally, scaffold cytotoxicity was characterized through live/dead staining on days 1 and 5 post-culture.

2.4.2. In Vivo Evaluation

All *in vivo* studies were conducted on a two-stage rat model, where rotator cuff repair was performed one week after the transection injury was induced. This two-stage process enhances model accuracy and control over experimental conditions, allowing for effective observation of the applied treatment's effects by minimizing inconsistencies and variability. Specifically, it helps reduce or eliminate the initial inflammatory response. DI-I labeled rBMSCs were seeded onto the SHAIPs and primed with 0.5 μ M HhAg for 4 days before implantation. The seeded SHAIPs were implanted between the tendon and bone in the right shoulder. Gene expression levels were evaluated separately for each sample on postoperative day 3 and then compared to *in vitro* controls, with day 0 being the time of implantation. Concurrently, the delivery of primed rBMSCs was assessed through histological analysis on postoperative day 3.

CHAPTER 3

RESULTS AND DISCUSSION

This section summarizes the stepwise progression of PCL SHAIPIs as a cell delivery platform in entheses regeneration from fabrication to cell-seeded scaffold evaluation. The preparation parameters for producing uniform gelatin microspheres using microfluidic emulsion were optimized, resulting in microspheres of 100-275 μm in diameter. Higher gelatin concentrations generated larger microspheres, and each trial yielded a considerable number of gelatin beads—sufficient to produce approximately 35 circular SHAIPIs, each 10 mm in diameter. These templating microspheres were connected via thermal annealing for 4 h at 80 °C, maintaining a consistent, well-defined microstructure. Gelatin templates infiltrated with 10% PCL in dichloromethane exhibited no signs of fragmentation upon template removal. PCL SHAIPIs characterized in subsequent cell studies featured a 190 μm scaffold pore size, with a window size and surface pore size of around 25.4% and 80%, respectively.

For cell-seeded scaffold characterization, no discernable signs of cytotoxicity were observed from live/dead staining, and Gli1 expression of the primed cell culture remained upregulated throughout the study duration. Furthermore, histological analysis showed the successful delivery of primed rBMSCs to the repair site *in vivo*, indicated by the presence of DI-I labeled rBMSCs following implantation. These results demonstrate the feasibility of PCL SHAIPIs as an effective cell delivery platform for HhAg-stimulated MSCs in entheses regeneration.

3.1. Gelatin Microsphere Preparation

The most uniform gelatin microspheres were obtained using 15-20% gelatin at 0.0375 and 0.75 mL/min for the discontinuous and continuous phase flow rates, respectively. Although the particle size can be modified by adjusting these flow rates, small changes can quickly disrupt sample uniformity. For example, at discontinuous phase flow rates above 0.05 mL/min, oval-shaped gelatin beads were produced. Instead, the particle size can be more precisely controlled by changing the discontinuous phase concentration, with higher gelatin concentrations generating larger bead sizes. Low polydispersity, highly uniform gelatin microspheres were obtained at these optimal flow parameters for 10-30% gelatin, corresponding to microspheres of 100-275 μm in diameter (Figure 3). For gelatin concentrations above 30%, however, the microfluidic device easily clogged or produced coalesced gelatin microspheres (Figure A1). Coalesced gelatin microspheres could be produced at lower gelatin concentrations by strongly agitating either the gelatin or toluene solutions to introduce air, where the dissolved gas interfered with fluid flow dynamics. Coalescence could be identified by the spontaneous increase in microsphere size, normally occurring within the first 3 min of microsphere production. Based on the microfluidic device setup, these coalesced beads reached around 550 μm in diameter, approximately doubling the expected microsphere size. Although the coalesced gelatin microspheres appear relatively uniform, their excessive size limits the clinical applicability of these beads, where smaller microspheres tend to be optimal. The risk of microsphere coalescence can be minimized by allowing both solutions to passively degas for at least 12 h with little to no agitation. Approximately 175-200 mL of the collection phase was added to a 250 mL Erlenmeyer flask for each trial, and decreasing this volume led to a rougher, irregular bead surface. Higher concentrations of gelatin microspheres in the collection phase increase the likelihood of beads colliding before fully stabilizing, causing defects or dents on the

microsphere surface. Once stabilized, however, the gelatin microspheres can be stored in methanol for months at room temperature without experiencing any significant changes or degradation.

The freeze-drying process reduced the size of the gelatin microspheres by approximately 20.1%. Despite this size reduction, each trial produced an ample number of dried gelatin beads sufficient for the fabrication of at least 35 circular SHAIPIs, each measuring 10 mm in diameter. This fabrication process can be easily scaled by simply increasing the experiment duration and collection phase volume, enabling the incorporation of these homogeneous gelatin microspheres across a wide range of applications such as drug delivery.

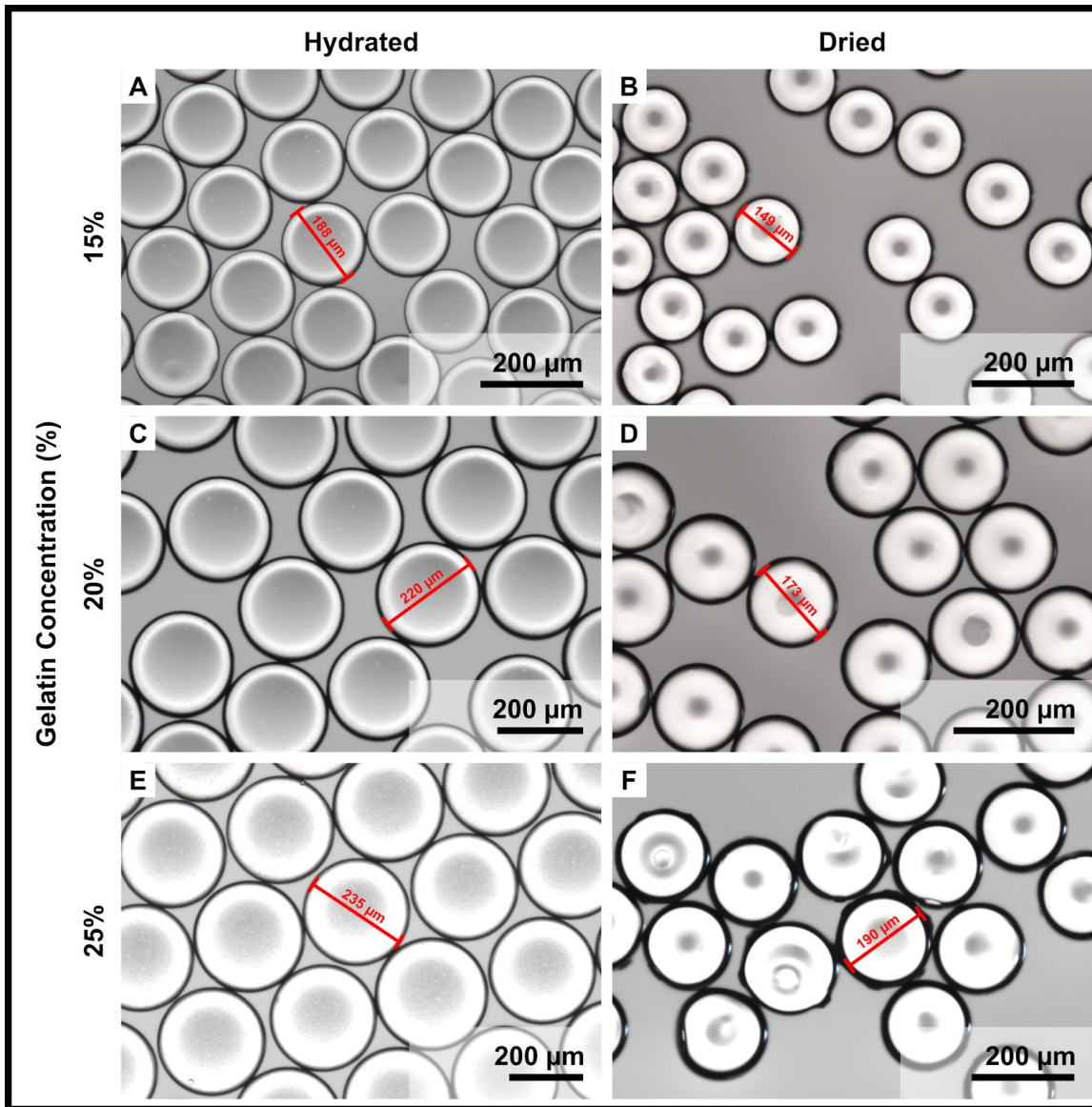


Figure 3. Optical micrographs of gelatin microspheres prepared using microfluidic emulsion at 0.0375 and 0.75 mL/min for the discontinuous (gelatin solution) and continuous (toluene with 3% span 80) phases, respectively. The figure shows the gelatin microspheres before (left) and after (right) drying under vacuum.

3.2. Gelatin Template Formation

Dried gelatin microspheres above 100 μm in diameter formed a hexagonal lattice after gently tapping for 3 min but templating extremely small microspheres resulted in undesirable gaps throughout the closely-packed lattice. Smaller microspheres require additional tapping time to assume this hexagonal arrangement. This method expands on the large-scale production of SHAIPs by simplifying setup requirements and restricting material use to readily available items in all standard laboratories. Notably, multiple templates could be formed simultaneously in a box oven, provided that the centrifuge tube racks were sufficiently spaced to prevent overcrowding. The window size, that is, the openings between pores in the scaffold structure, was determined by the original template pore size and the heating temperature during thermal annealing. Although the window size also increased with heating duration, this change was negligible, and instead, strongly depended on the heating temperature (Figure 4). Higher heating temperatures during the thermal annealing process correspond to larger window sizes, indicated by the size of connections between beads in the template structure. Compared to traditional inverse opal scaffold fabrication techniques, this modified approach required a significantly higher heating duration due to increased contact with the methanol environment. Despite leading to a heightened heating duration, the methanol is needed to prevent cracking from uneven heating or over drying, preserving template integrity and microstructure. The optimal heating duration was found to be 4 h, since other heating durations either induced minimal changes to the template structure or resulted in variable window sizes. Templates produced beyond this optimum remained largely unchanged and strongly attached to the centrifuge tube mold, unnecessarily increasing removal difficulty. Furthermore, while durable templates could often be collected after 3 h of thermal annealing, these templates exhibited low consistency in window size, varying between 1-5% relative to the expected window size at that heating

temperature. Gelatin templates produced at heating temperatures between 75-90 °C displayed the most well-defined structure and stability. Templates formed at lower heating temperatures frequently broke apart when handled, whereas templates produced at elevated heating temperatures readily fused together, permanently losing their microstructure. SHAIPIs for subsequent steps were fabricated from templates produced at 80 °C for 4 h, as they featured the highest consistency and were collected with minimal difficulty.

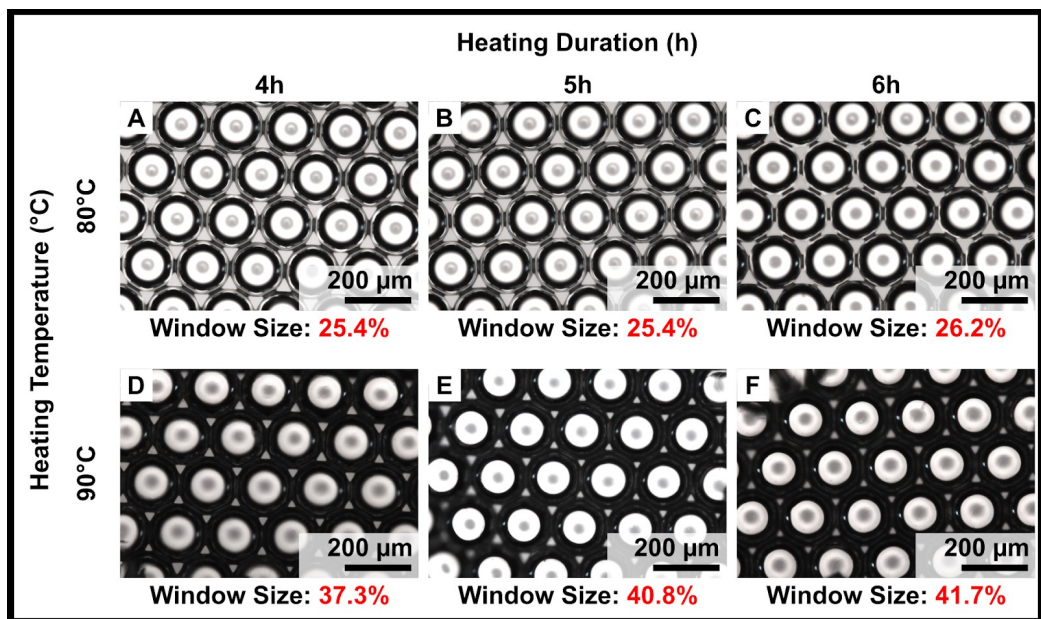


Figure 4. Optical micrographs illustrating changes in the window size resulting from thermal annealing at varying temperatures and heating durations.

3.3. SHAIPI Fabrication

Circular SHAIPIs with a pore size of 190 μm were obtained by templating with 195 μm microspheres, experiencing a slight size reduction after polymeric freeze-drying processes. These monolayer scaffolds possessed a highly ordered, uniform structure, characterized by a well-defined pore size and distribution (Figure 5). Although this

procedure is intended for SHAIP fabrication, the number of layers in the scaffold can be controlled by carefully adjusting the quantity of templating microspheres introduced into the centrifuge tube mold. Bilayer scaffolds were also fabricated using the same protocol (Figure A2). The infiltrating polymer concentration contributes to the mechanical properties, structural integrity, and pore interconnectivity, as the polymer concentration is crucial in determining the scaffold thickness. Higher polymer concentrations produced thicker, denser scaffolds that more accurately replicated the template structure; however, the polymer solution could struggle to fully penetrate the template void spaces. Excessive polymer concentration could also lead to the partial blockage of channels between pores, thereby reducing scaffold interconnectivity. The optimal balance of these key scaffold characteristics occurred between 10-20% PCL in dichloromethane. In this study, SHAIPs were produced using 10% PCL and exhibited robust physical capabilities and flexibility, enabling effective handling for use in ensuing cell studies. These SHAIPs possessed a large surface pore size of approximately 80% of the total scaffold pore size, enhancing nutrient diffusion and host integration. The surface pore size closely aligns with the infiltrating polymer concentration, following comparable trends to the scaffold thickness. For example, PCL concentrations above 25% resulted in the complete encapsulation of the scaffold despite efforts to remove excess polymer from the template surface. Conversely, PCL concentrations below 5% yielded scaffolds that struggled to maintain their structural integrity following template removal. While SHAIPs in this study were composed of PCL, other materials, such as PLGA, can be substituted for PCL due to the relatively gentle infiltration and template removal processes in this modified SHAIP fabrication procedure.

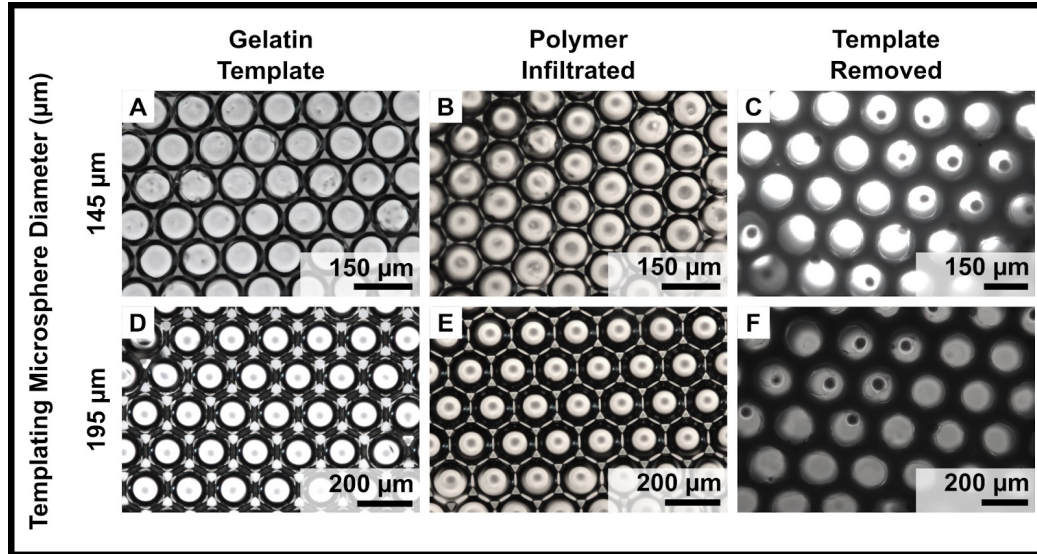


Figure 5. Optical micrographs showing the step-by-step SHAIp fabrication procedure for 145 and 195 μm gelatin microspheres, respectively.

3.4. *In Vitro* Evaluation

Cell viability for rBMSCs seeded into the PCL SHAIps was preserved through 5 days of culture, as evidenced by the absence of dead cells in the live/dead staining (Figure 6A). Therefore, these SHAIps exhibited little to no cytotoxicity and could support cell seeding. The HhAg-stimulated rBMSC-seeded SHAIps demonstrated increased Gli1 and Runx2 expression levels for 4 days of culture, with no changes observed on day 14 (Figure 6B). This increased expression of Gli1 indicated the successful upregulation of the Hh-signaling pathway and osteogenic transcription factor Runx2 which are crucial to proper entesis healing outcomes. Enhanced Gli1 expression promotes the differentiation of MSCs into osteogenic and chondrogenic lineages, facilitating the formation of a graded transition between the tendon and bone.^[23] The early, elevated expression of Runx2 without the upregulation of Sox9 and Scn suggested that the cells committed to the osteogenic lineage. Furthermore, a 50% decrease in the expression of SLRP proteins Dcn and Bgn was also reported on days 4 and 14 (Figure 6B). These

proteins are essential for ECM remodeling and fibrocartilage formation, and their decreased expression could enable more controlled, regulated wound healing. Existing literature indicates that decreased levels of Bgn and Dcn reduce excessive scarring and improve healing outcomes, with regenerated tissues exhibiting enhanced mechanical properties, without affecting the early healing response.^[25] This work revealed that primed rBMSCs remained viable when seeded into the PCL SHAIPIs, and their genetic expression profiles appeared similar to previously identified Gli1+ enthesis stem cells.

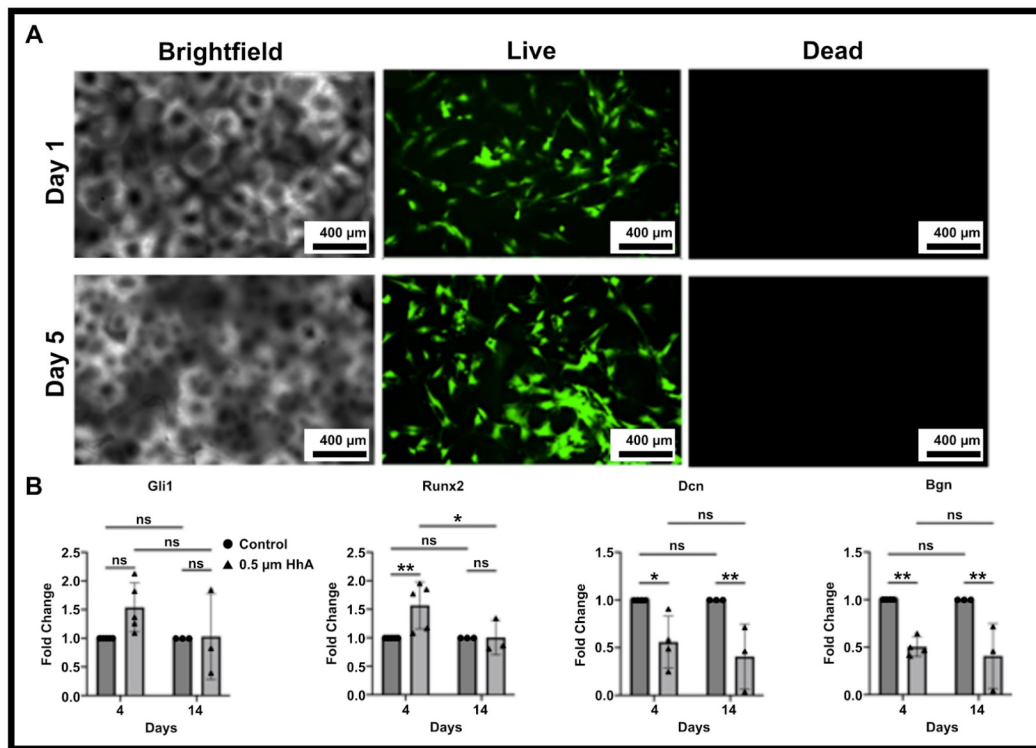


Figure 6. (A) Brightfield micrographs and fluorescence images of live/dead staining on days 1 and 5. (B) Comparison of *in vitro* gene expression levels for primed rBMSCs seeded into the PCL SHAIPIs to non-stimulated controls. The original images were provided by Dr. Stavros Thomopoulos, Columbia University.

3.5. *In Vivo* Evaluation

The successful delivery of primed rBMSCs *in vivo* was confirmed by the presence of DI-I labeled cells at the repair site 3 days postoperatively, as shown in the histological analysis (Figure 7A). Moreover, *in vivo* gene expression levels on postoperative day 3 closely mirrored the patterns observed during *in vitro* scaffold evaluation (Figure 7B). Both Gli1 and Runx2 expression levels elevated, while Dcn and Bgn expression levels declined. This data validated the applicability of PCL SHAIPIs as an effective cell delivery platform for primed rBMSCs in rotator cuff repair, maintaining high cell viability and upholding predicted cell behavior throughout the study duration.

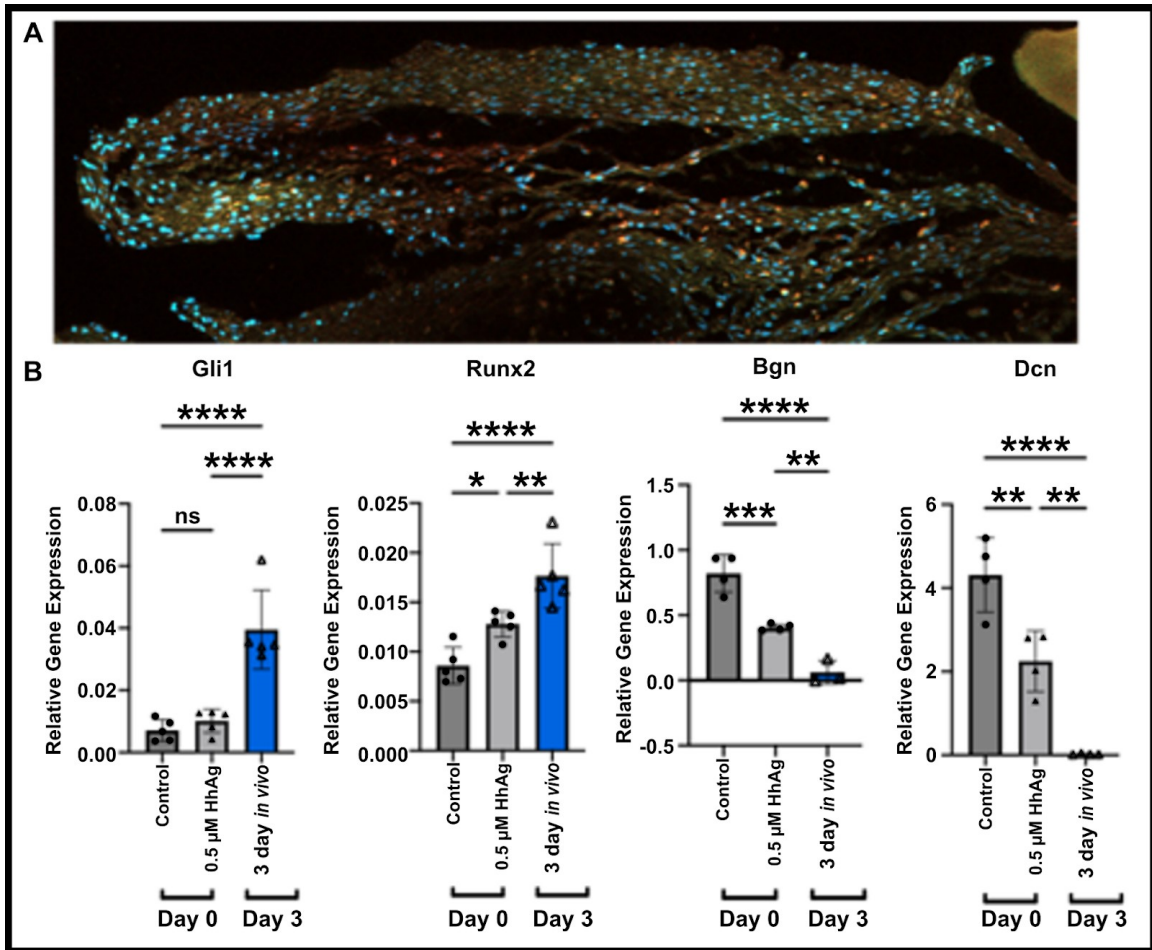


Figure 7. (A) Histological analysis of HhAg-stimulated rBMSCs *in vivo* (DI-I and Gli1 orange). (B) Comparison of *in vivo* gene expression levels for primed rBMSCs seeded into the PCL SHAPs to *in vitro* controls. The original images were provided by Dr. Stavros Thomopoulos, Columbia University.

CHAPTER 4

CONCLUSIONS

This study proposed and tested a modified SHAIIP fabrication procedure that enhances their clinical relevance by improving process scalability and simplicity. Although SHAIIPs possess a well-defined pore structure and high pore interconnectivity, these scaffolds remain relatively unexplored due to challenges in their production, requiring a specialized setup with limited experimental data available. This modified procedure requires only basic tools commonly available in most standard laboratories, and multiple SHAIIPs can be produced simultaneously, enabling the rapid fabrication of a statistically relevant number of samples. Unfortunately, a limitation of this approach relates to the size and shape of the resultant SHAIIPs, restricted to the 10 mm circular disk. Nevertheless, these scaffolds are typically sufficient for a variety of applications such as drug testing and disease modeling.

Preliminary data collected from cell-seeded scaffold evaluation highlights the feasibility of PCL SHAIIPs as a cell delivery platform for primed rBMSCs, retaining high cell viability and upregulation of the Hh-signaling pathway. These results align with improved healing outcomes for rotator cuff repair shown in Gli1+ enthesis stem cell treatment, promoting proper enthesis regeneration in lieu of scarring which is frequently observed in older populations. Further research, however, is needed to fully understand the benefits and regenerative capacity of this treatment.

CHAPTER 5

RECOMMENDATIONS

Adjustments to the polymer solution can be made to further enrich or enhance the functionality of the scaffold while optimizing the scaffold properties for various applications. Specifically, growth factors and other bioactive molecules can be included into the infiltrating polymer solution to guide cell growth and tissue maturation by leveraging the uniform release profile of an inverse opal scaffold. Alternatively, the inclusion of small microspheres, ranging from 10-20 μm , into the polymer solution can result in a hierarchical scaffold structure, creating supplementary pores that enhance cellular cross-talk and nutrient diffusion. The microsphere composition must not be affected by the scaffold material, removable without altering the scaffold structure.

Another method to augment SHAIIP performance is through surface modification which can promote cell adhesion and biocompatibility without compromising scaffold integrity. Surface modifications are an effective approach for enhancing SHAIIPs, given their high surface area-to-volume ratio. For example, microgrooves can be introduced onto the SHAIIP surface via laser engraving to elevate surface roughness, improving cell adhesion, recruitment, and scaffold integration. Implementing these strategies will greatly advance scaffold versatility and adaptability, increasing the likelihood of successful outcomes in future applications.

APPENDIX A
EXTRA FIGURES

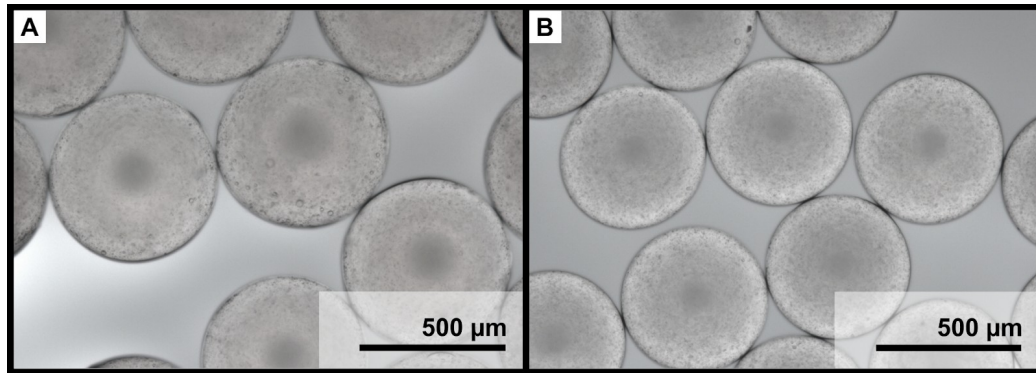


Figure A1. Optical micrographs of gelatin microspheres (A) before and (B) after drying under vacuum.

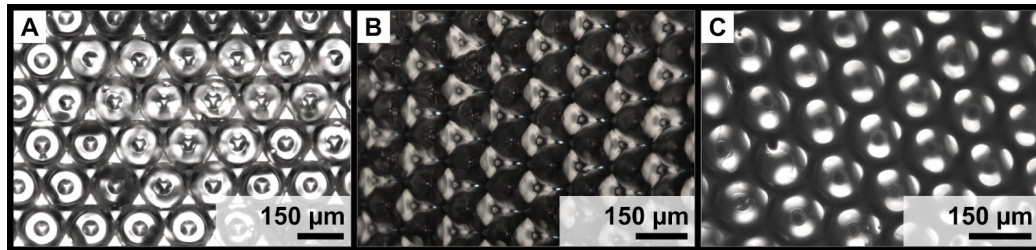


Figure A2. Optical micrographs showing the step-by-step fabrication of an inverse opal scaffold with a bilayer structure: (A) gelatin template, (B) template-containing scaffold, and (C) final scaffold.

REFERENCES

1. A. Koyyada, P. Orsu (2020) Recent advancements and associated challenges of scaffold fabrication techniques in tissue engineering applications. *Regenerative Engineering and Translational Medicine* 7(24), 147-159.
<http://dx.doi.org/10.1007/s40883-020-00166-y>
2. A. Eltom, G. Zhong, A. Muhammad (2019) Scaffold techniques and designs in tissue engineering functions and purposes: A review. *Advances in Material Science and Engineering* 2019.
<https://doi.org/10.1155/2019/3429527>
3. M.N. Collins, G. Ren, K. Young, S. Pina, R.L. Reis, J.M. Oliveira (2021) Scaffold fabrication technologies and structure/function properties in bone tissue engineering. *Advanced Functional Materials* 31(21).
<http://dx.doi.org/10.1002/adfm.202010609>
4. X. Zhang, X. Chen, H. Hong, R. Hu, J. Liu, C. Liu (2022) Decellularized extracellular matrix scaffolds: Recent trends and emerging strategies in tissue engineering. *Bioactive Materials* 10(1), 15-31.
<https://doi.org/10.1016/j.bioactmat.2021.09.014>
5. A.D. Pieri, Y. Rochev, D.I. Zeugolis (2021) Scaffold-free cell-based tissue engineering therapies: Advances, shortfalls, and forecast. *npj Regenerative Medicine* 6(1).
<http://dx.doi.org/10.1038/s41536-021-00133-3>
6. I.M. Adel, M.F. ElMeligy, N.A. Elkasabgy (2022) Conventional and recent trends of scaffold fabrication: A superior mode for tissue engineering. *Pharmaceutics* 14(2), 306.
<https://doi.org/10.3390/pharmaceutics14020306>
7. L. Suamte, A. Tirkey, J. Barman, P.J. Babu (2023) Various manufacturing methods and ideal properties of scaffolds for tissue engineering applications. *Smart Materials in Manufacturing* 1(4).
<https://doi.org/10.1016/j.smmf.2022.100011>
8. S. Choi, Y. Zhang, S. Thomopoulos, Y. Xia (2010) In vitro mineralization by preosteoblasts in PLGA inverse opal scaffolds reinforced with hydroxyapatite nanoparticles. *Langmuir* 26(14), 12126-12131.
<https://doi.org/10.1021/la101519b>

9. C. Zhu, S. Pongkitwitoon, J. Qiu, S. Thomopoulos, Y. Xia (2018) Design and fabrication of a hierarchically structured scaffold for tendon-to-bone repair. *Advanced Materials* 30(16).
<https://doi.org/10.1002/adma.201707306>
10. Y.S. Zhang, J. Yao, L.V. Wang, Y. Xia (2014) Fabrication of cell patches using biodegradable scaffolds with a hexagonal array of interconnected pores (SHAIPs). *Polymer* 55(1), 445-452.
<https://doi.org/10.1016/j.polymer.2013.06.019>
11. Y.S. Zhang, C. Zhu, Y. Xia (2017) Inverse opal scaffolds and their biomedical applications. *Advanced Materials* 29(33).
<https://doi.org/10.1002/adma.201701115>
12. B.P. Chan, K.W. Leong (2008) Scaffolding in tissue engineering: General approaches and tissue-specific considerations. *European Spine Journal* 17(4), 467-479.
<https://link.springer.com/article/10.1007/s00586-008-0745-3>
13. S.W. Choi, I.W. Cheong, J.H. Kim, Y. Xia (2009) Preparation of uniform microspheres using a simple microfluidic device and their crystallization into close-packed lattices. *Small* 5(4), 454-459.
<https://doi.org/10.1002/smll.200801498>
14. K.S. Park, C. Kim, J.O. Nam, S.M. Kang, C.S. Lee (2016) Synthesis and characterization of thermosensitive gelatin hydrogel microspheres in a microfluidic system. *Macromolecular Research* 24(6), 529-536.
<https://doi.org/10.1007/s13233-016-4069-6>
15. W. Weng, J. Chi, Y. Yu, C. Zhang, K. Shi, Y. Zhao (2021) Multifunctional composite inverse opal film with multiactives for wound healing. *ACS Applied Materials and Interfaces* 13(3), 4567-4573.
<https://doi.org/10.1021/acsami.0c20805>
16. L. Wang, L. Sun, F. Bian, Y. Wang, Y. Zhao (2022) Self-bonded hydrogel inverse opal particles as sprayed flexible patch for wound healing. *ACS Nano* 16(2), 2640-2650.
<https://doi.org/10.1021/acsnano.1c09388>
17. J. Xue, T. Wu, Y. Dai, Y. Xia (2019) Electrospinning and electrospun nanofibers: Methods, materials, and applications. *Chemical Reviews* 119(8), 5298-5415.
<http://dx.doi.org/10.1021/acs.chemrev.8b00593>

18. D. Ji, Y. Lin, X. Guo, B. Ramasubramanian, R. Wang, N. Radacsi, R. Jose, X. Qin, S. Ramakrishna (2024) Electrospinning of nanofibers. *Nature Reviews Methods Primers* 4(1).
<http://dx.doi.org/10.1038/s43586-023-00278-z>
19. Z. Gu, J. Fu, H. Lin, Y. He (2020) Development of 3D bioprinting: From printing methods to biomedical applications. *Asian Journal of Pharmaceutical Sciences* 15(5), 529-557.
<https://doi.org/10.1016/j.ajps.2019.11.003>
20. Y. He, Z. Gu, M. Xie, J. Fu, H. Lin (2020) Why choose 3D bioprinting? Part II: Methods and bioprinters. *Bio-Design and Manufacturing* 3(1), 1-4.
<http://dx.doi.org/10.1007/s42242-020-00064-w>
21. N.A. Trasolini, B.R. Waterman (2022) Rotator cuff repairs fail at an alarmingly high rate during long-term follow-up: Graft augmentation and biologics may improve future outcomes. *Arthroscopy* 38(8), 2413-2416.
<https://doi.org/10.1016/j.arthro.2022.04.002>
22. A.G. Schwartz, F. Long, S. Thomopoulos (2015) Enthesis fibrocartilage cells originate from a population of hedgehog-responsive cells modulated by the loading environment. *Development* 142(1), 196-206.
<https://doi.org/10.1242/dev.112714>
23. F. Fang, M. Casserly, J. Robbins, S. Thomopoulos (2025) Hedgehog signaling directs cell differentiation and plays a critical role in tendon enthesis healing. *npj Regenerative Medicine* 10(1).
<https://doi.org/10.1038/s41536-025-00392-4>
24. C. Zhu, J. Qiu, S. Thomopoulos, Y. Xia (2021) Augmenting tendon-to-bone repair with functionally graded scaffolds. *Advanced Healthcare Materials* 10(9).
<https://doi.org/10.1002/adhm.202002269>
25. T.P. Leahy, A.K. Fung, S.N. Weiss, N.A. Dymant, L.J. Soslowsky (2023) Investigating the temporal roles of decorin and biglycan in tendon healing. *Journal of Orthopaedic Research* 41(10), 2238-2249.
<https://doi.org/10.1002/jor.25590>